Continuum Mech. Thermodyn. (2016) 28:139–156
DOI 10.1007/s00161-014-0409-y

ORIGINAL ARTICLE

Antonio Cazzani · Marcello Malagù · Emilio Turco

Isogeometric analysis: a powerful numerical tool for the elastic analysis of historical masonry arches

Received: 12 September 2014 / Accepted: 8 December 2014 / Published online: 28 December 2014

Abstract We illustrate a numerical tool for analyzing plane arches such as those frequently used in historical masonry heritage. It is based on a refined elastic mechanical model derived from the isogeometric approach. In particular, geometry and displacements are modeled by means of non-uniform rational B-splines. After a brief introduction, outlining the basic assumptions of this approach and the corresponding modeling choices, several numerical applications to arches, which are typical of masonry structures, show the performance of this novel technique. These are discussed in detail to emphasize the advantage and potential developments of isogeometric analysis in the field of structural analysis of historical masonry buildings with complex geometries.

Keywords Masonry arches · NURBS · Isogeometric analysis · Curved Timoshenko beam

1 Introduction

In the last ten years, the so-called isogeometric approach was largely applied to various field of the mechanics. Starting from the seminal work [1], many extensions are contained in [2] and [3] and concern a wide range of problems such as vibrations and wave propagations, nearly incompressible solids, fluids, fluid-structure interaction. Isogeometric approach generalizes some ideas already used both in finite elements, see [4–7], and boundary elements [8,9] which use 2nd-order spline interpolation for displacements for finite elements and displacements and tractions for boundary elements.

The advantages of the isogeometric approach with reference to classical finite elements lie basically in the use of the same tools adopted by computer aided design (CAD), computer aided engineering (CAE) and computer aided manufacturing (CAM) and in the ability to represent in an exact way conic sections such as circles and ellipses. To better understand this issue, most software packages currently used for architectural design are precisely based on such CAD techniques. Hence, the ability to perform structural analyses on the same model used for design is extremely appealing. Up to now, however, researchers have concentrated most of their efforts on 2-D and 3-D continuum models or on shell-like structures [10–12]. Only recently some papers on 1-D problem appeared, even though they were particularly concerned on locking control, see [13–18].

Communicated by Prof. Victor Eremeyev, Prof. Peter Schiavone and Prof. Francesco dell'Isola.

A. Cazzani · M. Malagù
Dipartimento di Ingegneria Civile, Ambientale e Architettura (DICAAR), Università degli Studi di Cagliari, Cagliari, Italy
E-mail: antonio.cazzani@unica.it

M. Malagù
E-mail: marcello.malagu@gmail.com

E. Turco (✉)
Dipartimento di Architettura, Design e Urbanistica (DADU), Università degli Studi di Sassari, Sassari, Italy
E-mail: emilio.turco@gmail.com; emilio.turco@uniss.it

This suggests us to develop a curved Timoshenko beam element based on NURBS interpolation both for geometry and displacements. In [20], some details about the accuracy, the convergence and the computational cost of this approach are reported. Here, the focus is on technical examples which are meaningful from the architectural point of view. Some of them are inspired by famous historical building and are used to show the main features of the proposed approach. In particular, we investigate deformations and stresses in masonry arches. The presented results descend from the numerical simulation produced by the proposed theoretical model. Of course, the correspondence of such results to the behavior of existing structures (detected by means of field tests) can only be ascertained a posteriori. Therefore, based on a thrust line approach the presented method is used for a preliminary study on the stability of masonry structures. We highlight that buckling problem is not considered in this paper. Interested readers can found some insights in [21–24] and the papers cited therein.

The paper is organized as follows. First, we discuss, Sect. 2, the principal guidelines of the NURBS interpolation and the basic key points to build a mechanical model based on the isogeometric approach. Successively, some numerical results are presented and discussed in Sect. 3 to assess the performances of this numerical model. Finally, in Sect. 4, there are some concluding remarks and future developments.

2 Isogeometric model of plane curved beams with shear stiffness

Non-Uniform Rational B-Spline (NURBS) curves have been largely used in CAD, CAM and CAE for some decades. They constitute a smart way to construct lines, surfaces and solids which are somehow smooth. Essentially, the heart of the technology is based on the so-called Bézier curves (which take their name from this French engineer, working in the automotive industry Renault, who used them for the first time to design the shape of a car body) and have been precisely defined in 1959 by de Casteljau's recursive algorithm. By referring the interested reader to the specialized book [25] for an extended discussion of NURBS, both from theoretical and algorithmic point of view, here only the main key points will be outlined.

The starting point is the definition of a polynomial curve of order n by means of $n + 1$ control points which define the so-called control polygon, see Fig. 1. The most important characteristic of these curves is the invariance for affine transformation: Each isometric transformation, such as translation, rotation and reflection, can be applied to the curve simply applying it to the control points. The peculiar drawback of Bézier idea is the global nature of the interpolation: modifying one single control point changes the entire curve. This disadvantage is overcome by the B-spline concept: the curve is obtained joining several Bézier curves and preserving the desired continuity. As a consequence, each control point modifies only a part of the whole curve. However, B-splines cannot exactly represent circles or ellipses and, furthermore, they are non-invariant under a projective transformation. Conversely, NURBS, besides being invariant under projective transformations, are able to represent exactly conic sections, even those different from a parabola. This, in practice, is realized by assigning to each control point a weight which is able to *attract* the curve or to *push* it away with respect to the control point, as it is outlined in Fig. 1.

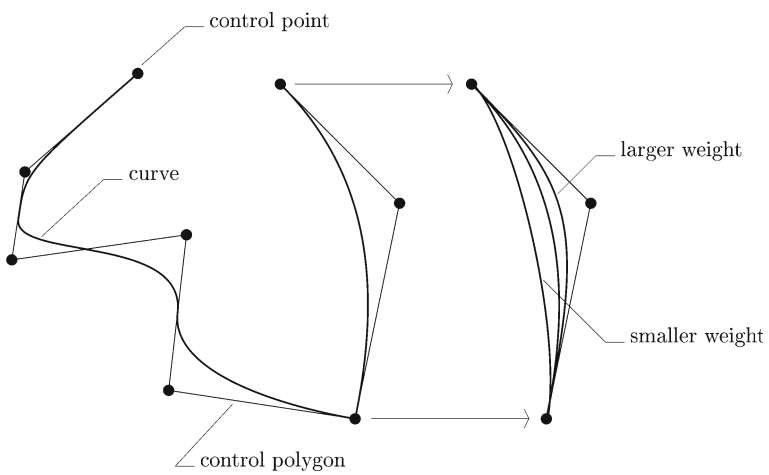

Fig. 1 NURBS basics: control points (•), control polygon, *curve* and control point weights influence

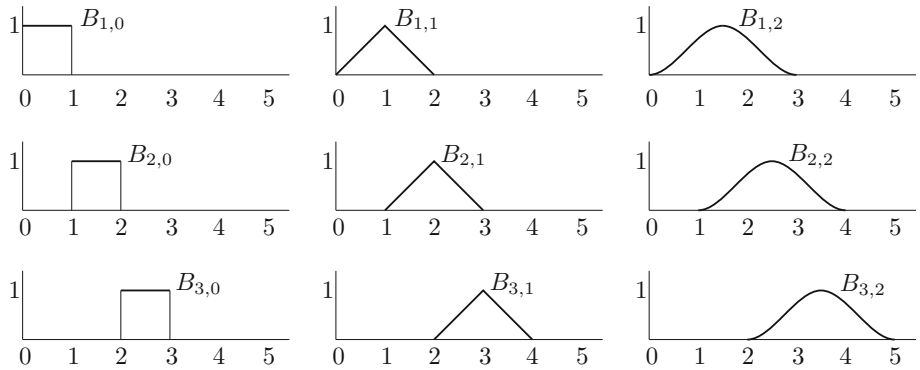

Fig. 2 B-spline bases up to 2nd order (on the abscissae there are knot indexes)

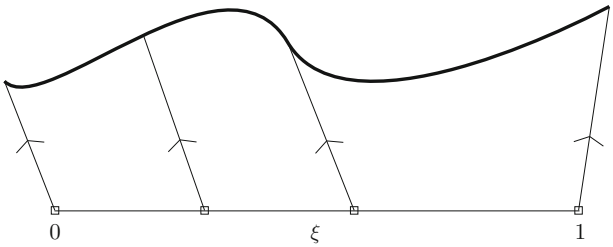

Fig. 3 NURBS basics: element subdivision and knots (□)

The keystone to build the numerical model is the NURBS representation of a curve. By referring to [25] for a systematic exposition on this issue, here, we recall only the bases useful to construct the numerical model. We say that a curve $\mathbf{x}$ has a p-degree NURBS representation when there exist $n \in \mathbb{N}$, control points $\mathbf{P}_i \in \mathbb{R}^3$, weights $g_i \in \mathbb{R}$, $i = 1, \ldots, n$, and a *knot vector*, i.e., a set $\boldsymbol{\Xi} = \{0 = \xi_1 \leq \xi_2 \leq \cdots \leq \xi_{n+p+1} = 1\}$ such that, for any $\xi \in [0; 1]$:

$$\mathbf{x}(\xi) = \sum_{i=1}^{n} R_{i,p}(\xi)\mathbf{P}_i, \tag{1}$$

where the NURBS basis $\{R_{i,p}(\xi)\}$ can be expressed as:

$$R_{i,p}(\xi) = \frac{B_{i,p}(\xi)g_i}{\sum_{i=1}^{n} B_{i,p}(\xi)g_i}, \tag{2}$$

in terms of B-splines bases $\{B_{i,p}(\xi)\}$ defined by the Cox-De Boor recursive formula (see also Fig. 2 for their graphical representation up to 2nd order):

$$B_{i,0}(\xi) = \begin{cases} 1 & \text{if} \quad \xi_i \leq \xi < \xi_{i+1} \\ 0 & \text{otherwise} \end{cases}, \tag{3}$$

$$B_{i,p}(\xi) = \frac{\xi - \xi_i}{\xi_{i+p} - \xi_i} B_{i,p-1}(\xi) + \frac{\xi_{i+p+1} - \xi}{\xi_{i+p+1} - \xi_{i+1}} B_{i+1,p-1}(\xi). \tag{4}$$

The so-called knot vector $\boldsymbol{\Xi}$ defines a partition of the parameter space [0; 1] similar to the classic finite element subdivision, see Fig. 3. Non-uniform knot vectors and repeated knots are the key ingredients of NURBS flexibility and produce refined geometric descriptions. Weights g_i related to ith control point enlarge the capabilities of the B-splines interpolation allowing also an exact representation of conic sections, see again Fig. 1.

Among all the properties of NURBS interpolations, the most interesting is the high degree of continuity. More precisely, each pth order function is of class C^{p-1}, i.e., it is continuous with its derivatives up to the $(p-1)$th order, and in particular, it is smooth on the inter-element boundaries (knots), but not on the NURBS

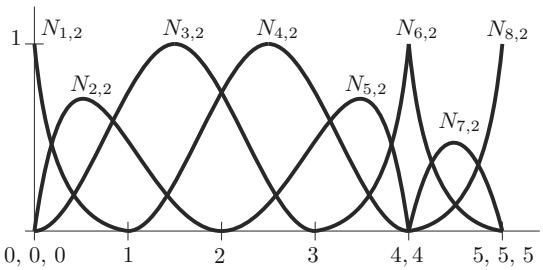

Fig. 4 NURBS control using repeated knots: lowering the continuity at the 4th knot for 2nd order NURBS (on the abscissa there are knot indexes)

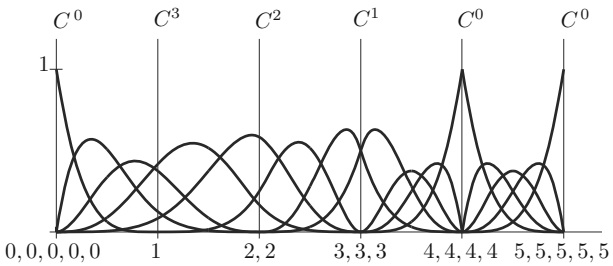

Fig. 5 NURBS control using repeated knots: lowering the continuity for 4th order NURBS. The resulting continuity order at all control points is also shown (on the abscissa there are knot indexes)

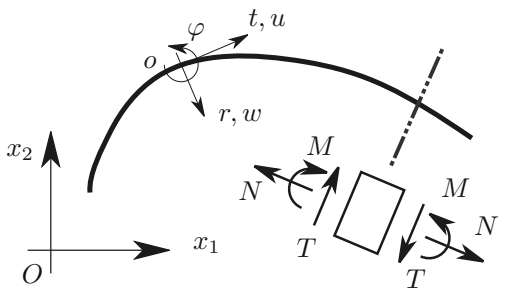

Fig. 6 Plane *curved* beam: *centroid line* and reference systems

boundaries (patch). However, if necessary, continuity degree can also be lowered by using repeated knots, see Figs. 4 and 5.

NURBS tools can be used to efficiently describe the geometry of a wide range of curves both in 2-D and 3-D. In order to build our numerical model, now we consider a curved plane beam (see Fig. 6) whose centroid line is a plane curve parametrized by the arc-length $s \in [0; \ell]$. We suppose also that one of the principal inertia axis and the shear center of the cross-section lie in the same plane. Let the global reference system be denoted by $(O; x_1, x_2)$ and the local one by $(o; t, r)$, t and r being, respectively, the tangent and the normal unit vectors to the curve. Moreover, we denote by R the curvature radius and by $(\cdot)'$ the derivatives with respect to the arc-length s. With this notation, the differential form of equilibrium and kinematic compatibility equations describing the curved Timoshenko plane beam problem in the local reference system are:

$$N' - \frac{T}{R} + q_t = 0, \quad T' + \frac{N}{R} + q_r = 0, \quad M' - T + m = 0, \tag{5}$$

$$\varepsilon = u' - \frac{w}{R}, \quad \gamma = w' + \frac{u}{R} + \varphi, \quad \chi = \varphi' . \tag{6}$$

Here, N, T and M denote the generalized stresses (axial and shear force and bending moment, see Fig. 6 for the definition of positive quantities) and q_t, q_r and m the generalized external forces per unit length (tangent and radial forces and distributed couples). In the local reference system, u and w are the displacements of the axis line and φ the section rotation while ε, γ and χ denote the generalized strains (axial, shear and curvature bending).

When the ratio h/R is small enough (h being the depth of the cross-section) the strain energy is practically indistinguishably from that derived from de Saint-Venant approach for a straight beam:

$$\phi = EA\varepsilon^2 + EI\chi^2 + GA^*\gamma^2. \tag{7}$$

Here, the above-mentioned definition of the strain energy has been used, while a more complete discussion on this topic will be presented in a forthcoming paper, see [19].

The curved beam problem can now be set in an equivalent variational formulation, such as the classical principle of total potential energy, which is certainly more suitable for a solution strategy based on finite elements:

$$\underset{u,w,\varphi}{\arg\min} \left\{ \frac{1}{2}\int_0^\ell \phi \mathrm{d}s - \int_0^\ell (q_t u + q_r w + m\varphi)\mathrm{d}s \right\}. \tag{8}$$

The main idea of the isogeometric approach is to exactly describe the geometry of the problem by NURBS interpolation and to use the same interpolating basis to represent the generalized displacements:

$$u(\xi) \approx \sum_{i=1}^{n} R_{i,p}(\xi)u_i, \quad w(\xi) \approx \sum_{i=1}^{n} R_{i,p}(\xi)w_i, \quad \varphi(\xi) \approx \sum_{i=1}^{n} R_{i,p}(\xi)\varphi_i, \tag{9}$$

by means of control points u_i, w_i, and φ_i.

Using the dot to denote the derivatives with respect to ξ and denoting by J the Jacobian of the transformation, we have:

$$J = \dot{s} = \sqrt{\dot{x}_1^2 + \dot{x}_2^2}, \quad R = \frac{J^3}{|\dot{x}_1\ddot{x}_2 - \ddot{x}_1\dot{x}_2|}, \tag{10}$$

thus, the generalized strains take the form:

$$\varepsilon = \frac{\dot{u}}{J} - \frac{w}{R}, \quad \gamma = \frac{\dot{w}}{J} + \frac{u}{R} + \varphi, \quad \chi = \frac{\dot{\varphi}}{J}. \tag{11}$$

Finally, problem (8) can now be discretized as:

$$\underset{u,w,\varphi}{\arg\min} \left\{ \frac{1}{2}\sum_{e=1}^{n_e}\int_{\xi_e}^{\xi_{e+1}} \phi_e J \mathrm{d}\xi - \int_{\xi_e}^{\xi_{e+1}} (q_t u + q_r w + m\varphi) J \mathrm{d}\xi \right\}. \tag{12}$$

where n_e is the number of subdivision of the parameter space. Enforcing (12) produces a linear system of algebraic equations whose unknowns are the values of the control point parameters u_i, w_i and φ_i, which completely define the deformed shape of the beam.

To set up the stiffness matrix and the load vector, it is necessary to evaluate some integrals. This task can be performed numerically by using the Gauss quadrature rule, even if the integrand functions are somewhat different from polynomials. Some guidelines about the number of Gauss points to be used for an efficient quadrature, can be deduced from [3] and from [20].

3 Numerical results

Here, the numerical results which are relevant to some arches, having a sound architectural and technical interest, are presented. For each arch, the deformed shape of the centroidal axis along with the diagrams of axial, shear and bending stresses and strains and the thrust line (referred to the arch outline) are shown: All these follow from an elastic analysis, where masonry is considered equally reacting to compressive and tensile stresses. All computations have been performed assuming constant values for material parameters. However, the code can deal with material parameters whose values are variable, provided their position dependence is known.

It should be emphasized that according to Heyman's *safe theorem* [26–28], an elastic analysis provides acceptable results in term of the thrust line only if such line strictly lies within the strip enclosed between the

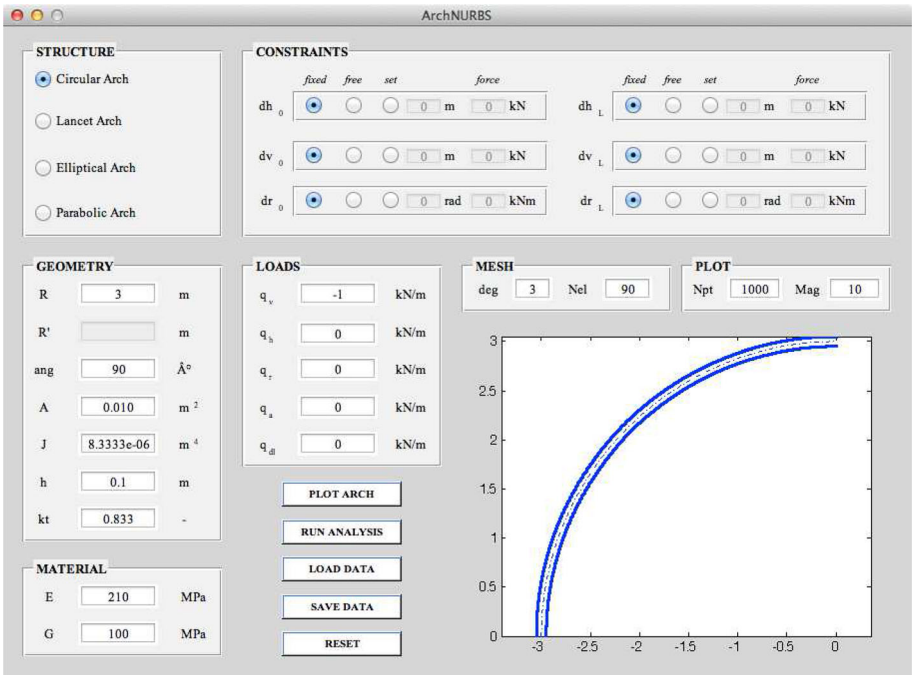

Fig. 7 Graphical user interface of the Arch-NURBS code

intrados and the extrados; otherwise, a limit analysis explicitly accounting for the no-tension material nature of masonry is required.

In general, therefore, the safety of an arch cannot be established by an elastic analysis only; however, if an elastic analysis provides an acceptable thrust line, then this is sufficient to ensure that for the given load condition the arch is safe. A deeper discussion of these and other issues for the assessment of the mechanical response of historic masonry buildings can be found in [29] and in [30]. Different arch examples can be found, instead, in [20]. There results are compared with analytical solutions and the output of other finite elements already presented in technical literature.

For all numerical tests an ad hoc developed MATLAB code has been used, whose graphical user interface is shown in Fig. 7. It is essentially based on NURBS algorithms reported in [25] (and later coded in a NURBS library) and on the GeoPDEs library, see [31]. The code is able to treat both arches having one of the most usual shapes, such as the circular, lancet, elliptic, parabolic one and arches whose geometry can be user-defined by means of control points in a standard DXF format. Particularly, attention has been paid to the interface in order to make simple each data modification allowing an easy use in a design process.

3.1 A circular arch

For the first test, one of the circular arches of the nave of Saint Saturnino church in Cagliari, Sardinia is considered. Figure 8 shows a view of the church facade (a) and of the considered arch (b) which can be exactly located from the plan (c) and the longitudinal cross-section (d) which are reported in the same figure.

The underlying St. Saturnino arch was accurately studied both from a geometric and mechanical point of view. It is characterized by an inner radius $R_i = 1.67$ m, an outer radius $R_e = 2.03$ m and a thickness $d = 0.70$ m, see Fig. 9. It is formed by yellow limestone blocks whose properties are: Young's modulus $E = 65$ GPa and Poisson's ratio $\nu = 0.1$. A vertical uniformly distributed load $q_v = 243$ kN/m, deriving for an accurate load analysis, has been considered besides the dead load of the arch and of the spandrel. Both of them are based on a mass-density $\rho = 2{,}300\,\text{kg/m}^3$.

In order to select the number of elements and the degree of the NURBS, we can look at some results presented in [20]. It turns out, in particular that for a semicircular arch subjected to a vertical distributed load, 16 elements of 4th order are sufficient to reduce to less than 0.1 % the error on the generalized stresses; the error on displacements is, of course, much less, since the adopted model relies on a displacement-based

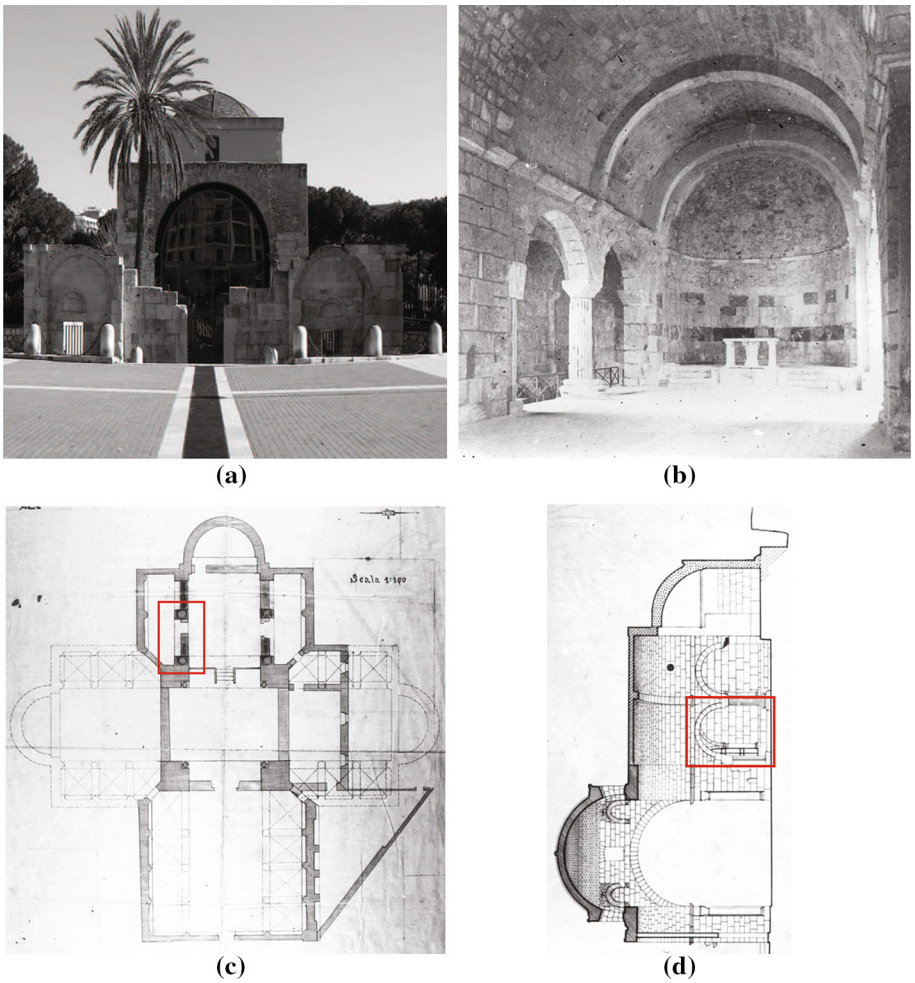

Fig. 8 Church of Saint Saturnino, Cagliari (Sardinia): front view (**a**), circular arches (**b**), plan (**c**) and cross-section (**d**)

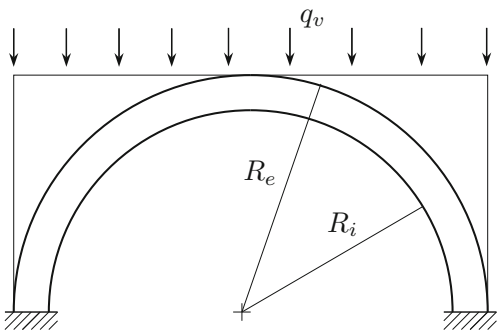

Fig. 9 Circular arch from the church of Saint Saturnino: the adopted structural scheme

formulation. Therefore, we use this mesh for the Saint Saturnino arch. Figure 10 reports a plot of the deformed shape of the centroid line superimposed to the undeformed one (a) and generalized strains ε, γ and χ (b), while Fig. 11 reports generalized stresses N, T and M (a) and the thrust line (b). From the analysis, we point out that the vertical displacement of the keystone is 0.22 mm; the normal force N lies in the range $-484.40\,\text{kN} \leq N \leq -246.07\,\text{kN}$ (i.e., it is always a compressive one); the shear force T varies between -246.69 and 246.69 kN and the bending moment is such that $-79.045\,\text{kNm} \leq M \leq 44.309\,\text{kNm}$. Finally, we note that the thrust line lies always inside the region bounded by the intrados and the extrados of the arch.

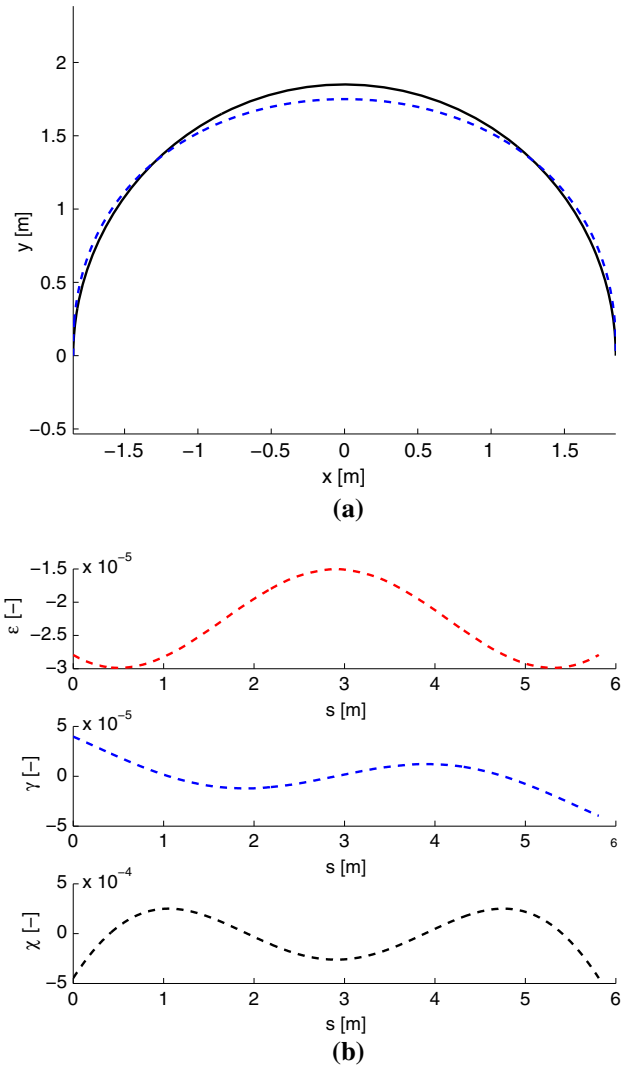

Fig. 10 Circular arch from the church of Saint Saturnino: displacements (**a**) and strains (**b**)

3.2 A lancet arch

We also consider a lancet arch typical of the gothic architecture such as, for example, one of those appearing in the cloister of the Department of Architecture of the University of Cagliari, see Fig. 12a. The structural scheme is reported in Fig. 12b. Geometry of the lancet is defined by the measured span $s = 1.71$ m and raise $r = 1.35$ m. The rectangular cross-section has depth $h = 0.4$ m and thickness $d = 0.4$ m. For the yellow limestone blocks, the assumed properties are: Young's modulus $E = 65$ GPa and Poisson's ratio $\nu = 0.1$. A vertical uniformly distributed load was evaluated by means of an accurate load analysis giving $q_v = 24$ kN/m, besides the dead load of the arch and of the spandrel which were both based on a mass-density $\rho = 2{,}550$ kg/m^3 and 2,450 kg/m^3, respectively.

With these data, the lancet arch was analyzed using a mesh of 32 NURBS elements of the 3rd order. This choice descends, as it is usual, by a convergence analysis performed both on displacements and generalized stresses taking into account only the dead load, for which an analytical solution exists, see [20]. Indeed, for these mesh the error on the displacements is less than 0.0001 % while the errors on generalized stresses are less than 0.4 %.

Figure 13 reports, in a graphical way, displacements (a) and generalized strains ε, γ and χ (b) while Fig. 14 reports the generalized stresses N, T and M (a) and the thrust line (b). We underline a negligible vertical displacement of the keystone, which is less 0.01 mm, a maximum compressive normal force equal to

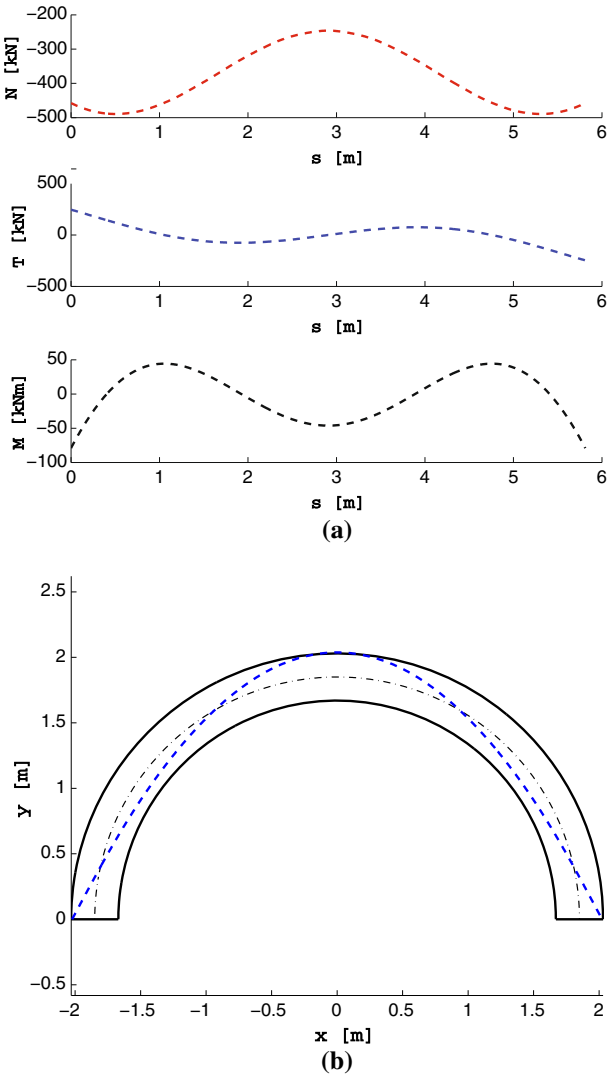

Fig. 11 Circular arch from the church of Saint Saturnino: stresses (**a**) and *thrust line* (**b**)

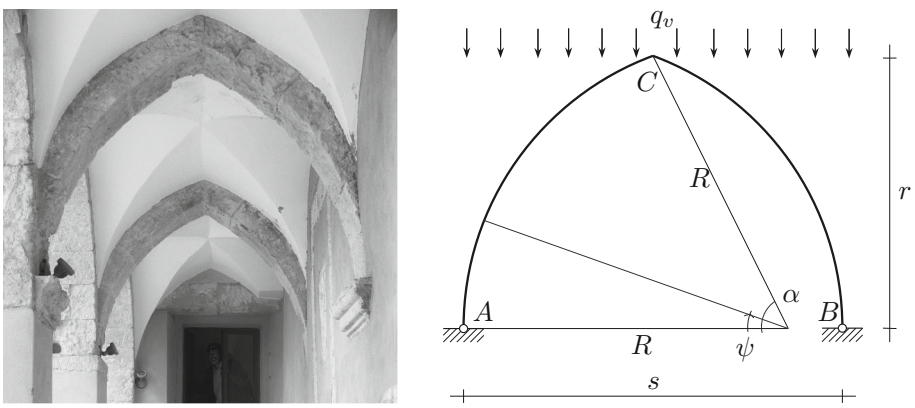

Fig. 12 Lancet arch: view of the cloister (**a**) and structural sketch (**b**)

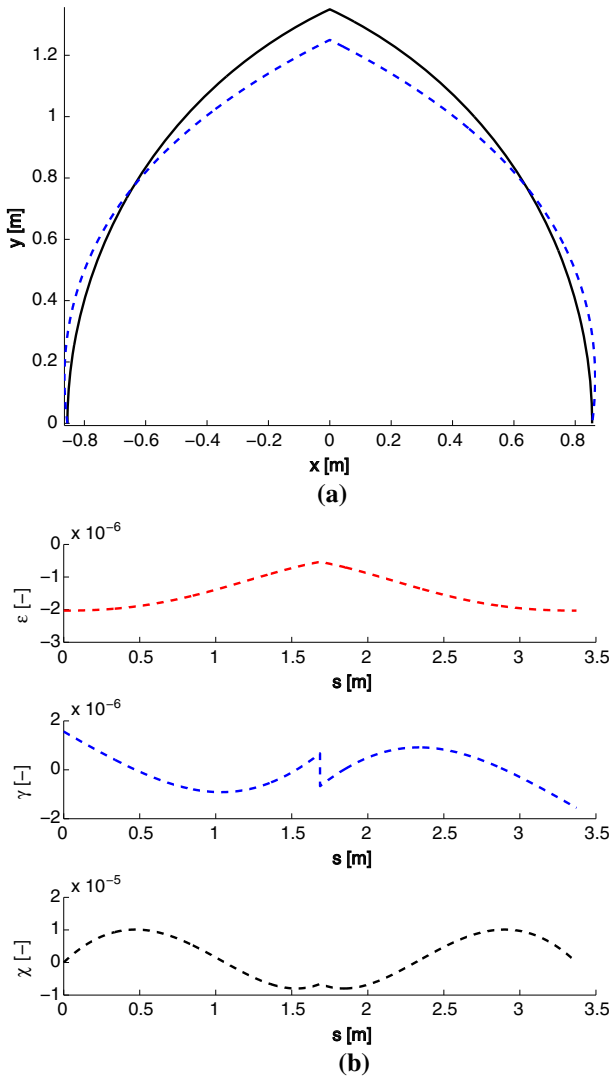

Fig. 13 Lancet arch: displacements (**a**) and strains (**b**)

21.103 kN while the shear force varies between −6.159 and 6.159 kN. The bending moment lies in the range between −1.1085 and 1.400 kNm. Finally, we note that the thrust line is really close to the centroid line, and this shows how effective are, from the viewpoint of structural design, lancet arches in Gothic architecture.

3.3 A parabolic arch

The test is inspired by one of the arches sustaining the roof in the loft of Milà house (also known as "la Pedrera"), one of the most famous creation by Gaudí, see Fig. 15a.

Following the descriptions of [32] and of [33] and referring to Fig. 15b for the structural scheme, the geometric data used to study this arch are: $R = 2.8$ m and $R' = 2.9$ m. For the constitutive parameters, we have assumed those available in technical literature to brick masonry, i.e., Young's modulus $E = 30$ GPa and Poisson's ratio $\nu = 0.15$. The rectangular cross-section of the arch is assumed to be 0.50 m (depth) by 0.10 m (thickness). The arch was analyzed for dead load and spandrel load based on a mass-density $\rho = 1{,}800\,\text{kg/m}^3$ and a vertical load $q_v = 50$ kN/m. We remarks that these data are not derived from an accurate load analysis but were only estimated.

A convergence analysis, not reported here for the sake of brevity, suggests the use of 4th order NURBS and 16 finite elements.

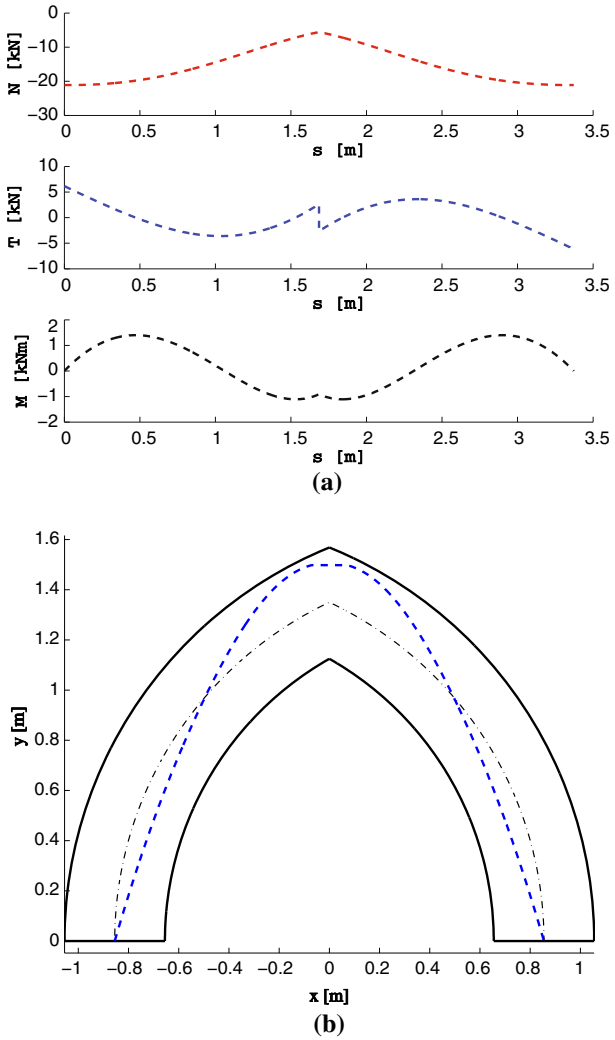

Fig. 14 Lancet arch: stresses (**a**) and *thrust line* (**b**)

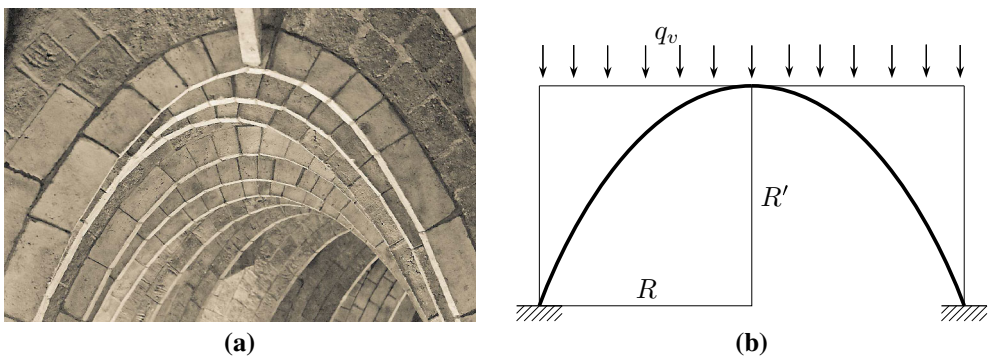

Fig. 15 Parabolic arch from Milà house: the arch (**a**) and the corresponding structural scheme (**b**)

Figure 16 reports, as before, a plot of displacements (a) and generalized strains ε, γ and χ (b) while Fig. 17 reports generalized stresses N, T and M (a) and the thrust line (b). In this case, we note that the maximum value of the axial force is $N_{\max} = -163$ kN while shear force is practically negligible. The bending moment is somewhat small, too. The thrust line runs close to the centroid line of the parabolic arch, as it is expected, since

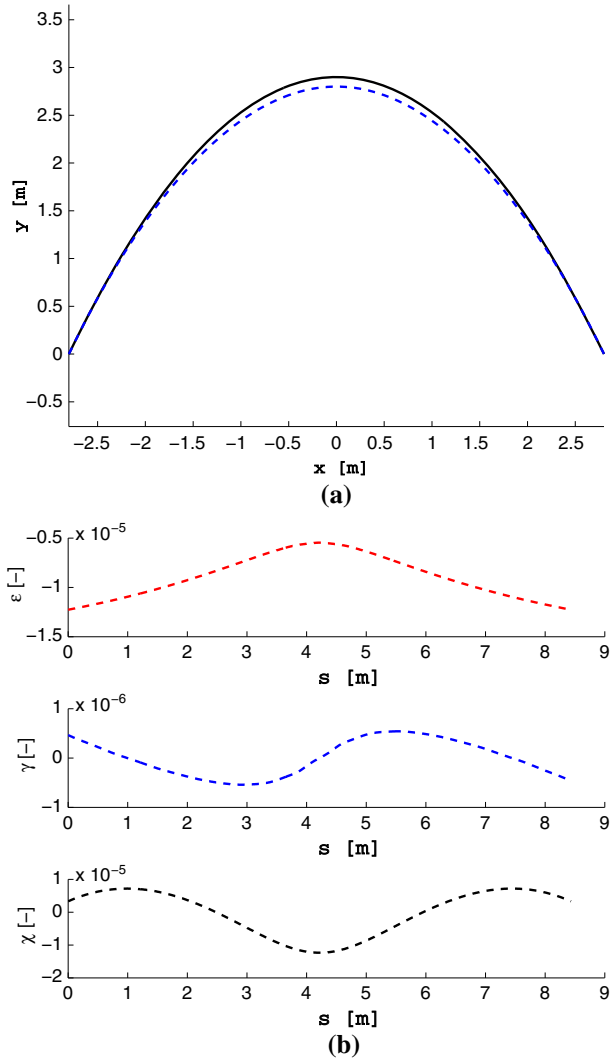

Fig. 16 Milà house arch: displacements (**a**) and strains (**b**)

the parabola is the funicular line for a uniformly distributed load along the projection of the span. Furthermore, as indicated in Fig. 16, the displacements are small. Indeed, the maximum vertical component is about 0.05 mm.

It is somehow interesting to compare, for the same values of loads and mechanical properties, the behavior of this parabolic arch with that of a circular arch having the same span. Figure 18 shows the generalized stresses, (a), and the thrust line, (b), for the equal span circular arch. It is clear that although the axial force is comparable in both cases, the shear force is now about fortyfold larger, while the bending moment, which is about tenfold larger, produces a thrust line somewhat far from the centroid line. In particular, at the keystone it lies out of the cross-section boundary.

3.4 An ogee arch

Finally, we consider the structural scheme of an ogee arch, like that depicted in Fig. 19, along with its construction rules, based on four equal equilateral triangles which are completely defined by the main geometric parameter R. The used data are $R = 1\,\text{m}$ and a rectangular cross-section having depth $h = 0.3\,\text{m}$ and thickness $b = 1\,\text{m}$. The material data are those corresponding to a typical sandstone, i.e., Young's modulus $E = 65\,\text{GPa}$ and Poisson's ratio $\nu = 0.15$. A concentrated load $F = 20\,\text{kN}$ applied at the keystone, a uniformly

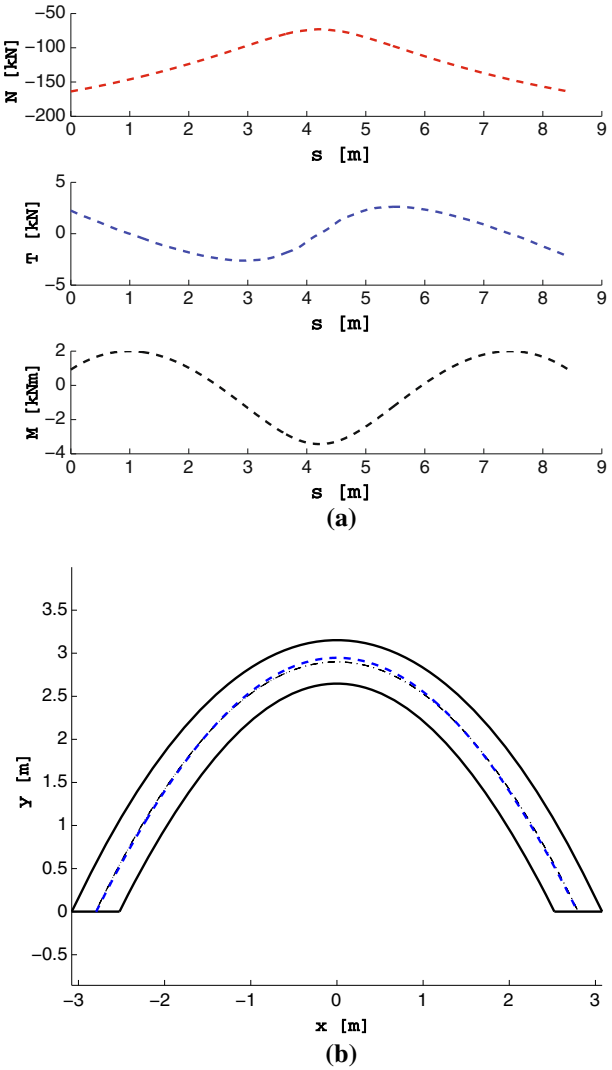

Fig. 17 Milà house arch: stresses (**a**) and *thrust line* (**b**)

distributed vertical load $q_v = 10\,\text{kN/m}$ and a dead load corresponding to a mass-density $\rho = 2{,}300\,\text{kg/m}^3$ are simultaneously acting on the arch.

For this problem, a reference solution is not available and so it was studied by means of a convergence analysis, which ensured that results in terms of both displacements and generalized stresses are stable by using 8 elements based on 5th order NURBS on one-half of the arc, when symmetry is accounted for.

In Fig. 20, displacements (a) and generalized strains (b), and in Fig. 21, generalized stresses (a) and the thrust line (b), for one-half of the ogee arch are, respectively, reported. From these plots, we observe that the maximum value of the compressive axial force N is equal to 37.976 kN while that of the shear force T (occurring at the impost) is 18.640 kN; the bending moment range goes from -1.7925 to 4.5413 kNm leaving the thrust line close to the centroid line. Displacements are negligible, since the vertical component at the keystone is less than 0.01 mm.

4 Concluding remarks

A quick tool for the elastic analysis of plane arches has been presented. The model is based on the isogeometric approach and provides the full advantages that such kind of interpolation, both for geometry and displacements, exhibits, viz. a high accuracy due to the refined representation of the geometry. Displacements, generalized

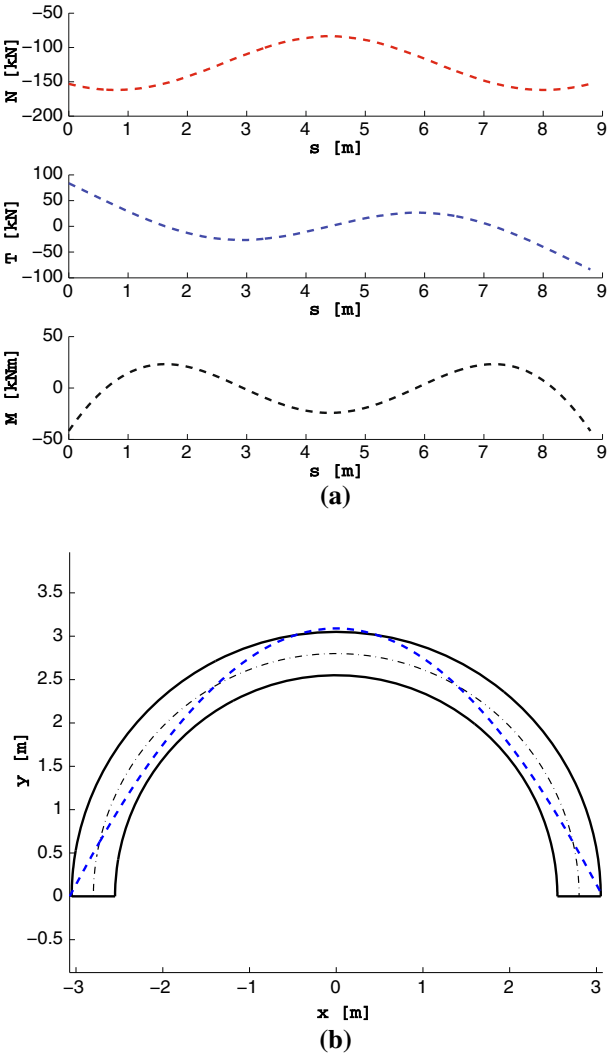

Fig. 18 Circular arch having the same span (and subjected to the same load condition) as the parabolic arch of Milà house: stresses (**a**) and *thrust line* (**b**)

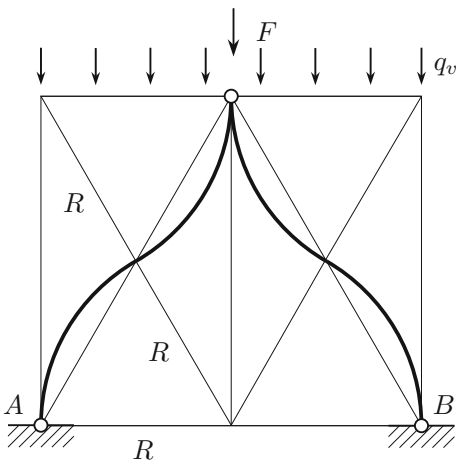

Fig. 19 Structural scheme of an ogee arch

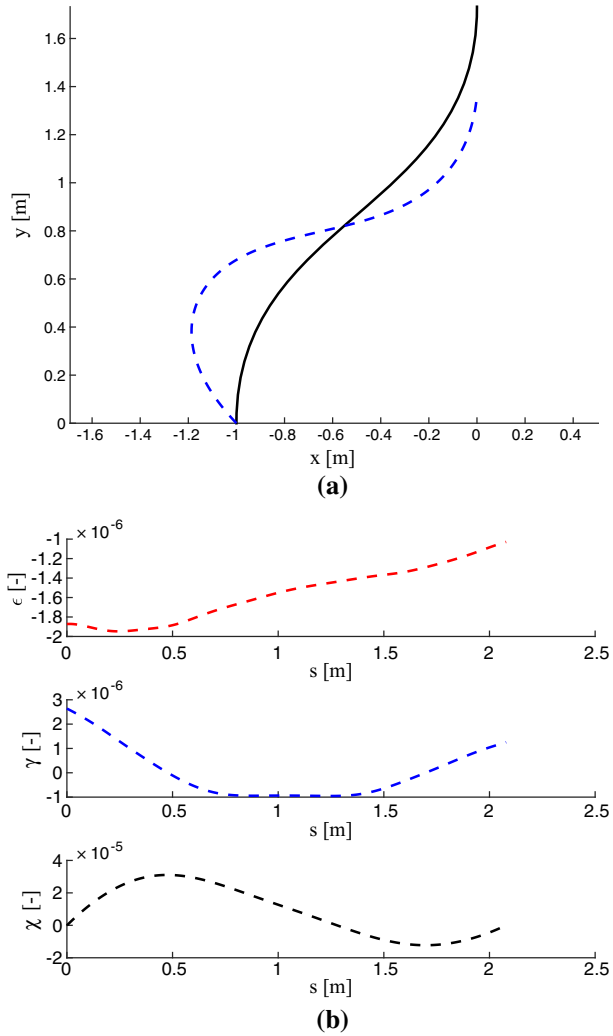

Fig. 20 Ogee arch: displacements (**a**) and strains (**b**)

stresses and thrust line can be calculated and represented in graphical way in a snap. This feature is particularly useful for interactive design and is particularly suitable when dealing with structural rehabilitation problems in historical buildings.

The thrust line representation is particularly suggestive since, thanks to the *safe theorem* proposed by Heyman [26–28], it is a powerful tool for analyzing and understanding the structural behavior of arches (see [34–36]). Indeed, it ensures that from the statics point of view, an arch is safe as long as, for the given load condition, a thrust line can be constructed which entirely lies within the depth of the arch, i.e., within the strip delimited by intrados and extrados.

In the present paper, only thrust-lines provided by elastic analyses have been presented; this is, however, a standard first step in the study of any arch. A more general framework which encompasses also limit analysis and reinforcement techniques based on Fiber-Reinforced Polymers (FRP), and which can be thought of as a further step in the study of arch response to loading, is being developed in [37].

Possible future developments concern:

- the generalization to 2D problem such as vaults or domes;
- the development of an interface which can produce a valid input file for the ArchNURBS code starting from the geometric data obtained by modern laser-scanner techniques;
- the model improvement, for example using a suitable damage parameter [38–42] taking into account that in some cases, it leads to non-unique and non-stable solutions, see [43–45]. Alternatively, there is the way proposed in [46,47], where a two-dimensional model for an interfacial zone is introduced, and this could be

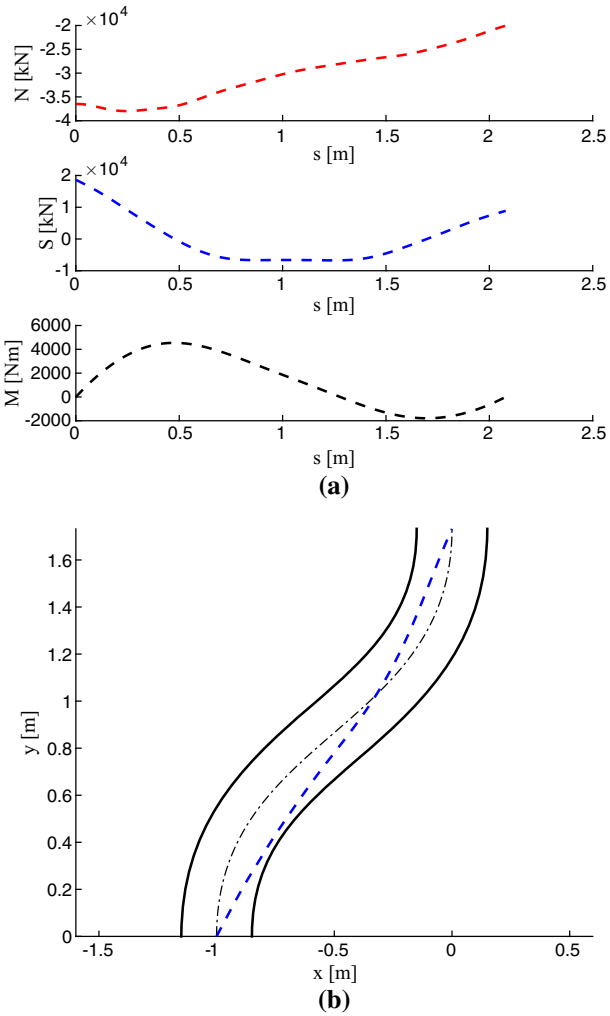

Fig. 21 Ogee arch: stresses (**a**) and *thrust line* (**b**)

used to describe more carefully concentrated damages. Furthermore, the variational techniques presented in [48], being adapted to dissipative phenomena, may be of use in this context. Finally, it seems attractive the use of higher continuum models as those described in [49–52];

- the damage detection using for example the procedure proposed by [53,54] which uses traveling loads as a signal;
- the extension to plasticity for evaluating collapse load, see for example [55–60].

Acknowledgments The financial support of RAS, the Autonomous Region of Sardinia, under Grant number F71J09999350002-CRP1_475 (Legge Regionale 7/2007, bando 2008, Progetto *MISC: Metodi Isogeometrici per Strutture Curve*) is gratefully acknowledged. The authors wish to gratefully recognize the cooperation of the Preservation Office, *Soprintendenza BAPSAE per le Province di Cagliari e Oristano*, for accessing the archival documents, photographs and drawings, which are relevant to the church of Saint Saturnino, and for authorizing their reproduction here.

References

1. Hughes, T.J.R., Cottrell, J.A., Bazilevs, Y.: Isogeometric analysis: CAD, finite elements, NURBS, exact geometry and mesh refinement. Comput. Methods Appl. Mech. Eng. **194**, 4135–4195 (2005)
2. Cottrell, J.A., Hughes, T.J.R., Bazilevs, Y.: Isogeometric Analysis: Toward Integration of CAD and FEA. Wiley, New York (2009)
3. Hughes, T.J.R., Reali, A., Sangalli, G.: Efficient quadrature for NURBS-based isogeometric analysis. Comput. Methods Appl. Mech. Eng. **199**, 301–313 (2010)

4. Aristodemo, M.: A high continuity finite element model for two-dimensional elastic structures. Comput. Struct. **21**, 987–993 (1985)
5. Bilotta, A., Formica, G., Turco, E.: Performance of a high-continuity finite element in three-dimensional elasticity. Commun. Numer. Methods Eng. **26**(9), 1155–1175 (2010)
6. Benedetti, A., Tralli, A.M.: A new hybrid F.E. model for arbitrarily curved beam—I. Linear analysis. Comput. Struct. **33**(6), 1437–1449 (1989)
7. Echter, R., Bischoff, M.: Numerical efficiency, locking and unlocking of NURBS finite elements. Comput. Methods Appl. Mech. Eng. **199**(5–8), 374–382 (2010)
8. Aristodemo, M., Turco, E.: Boundary element discretization of plane elasticity and plate bending problems. Int. J. Numer. Methods Eng. **37**, 965–987 (1994)
9. Turco, E., Aristodemo, M.: A three-dimensional B-spline boundary element. Comput. Methods Appl. Mech. Eng. **155**, 119–128 (1998)
10. Benson, D.J., Bazilevs, Y., Hsu, M.C., Hughes, T.J.R.: Isogeometric shell analysis: the Reissner–Mindlin shell. Comput. Methods Appl. Mech. Eng. **199**, 276–289 (2010)
11. Benson, D.J., Bazilevs, Y., Hsu, M.-C., Hughes, T.J.R.: A large deformation, rotation-free, isogeometric shell. Comput. Methods Appl. Mech. Eng. **200**(13–16), 1367–1378 (2011)
12. Kiendl, J., Bletzinger, K.-U., Linhard, J., Wüchner, R.: Isogeometric shell analysis with Kirchhoff–Love elements. Comput. Methods Appl. Mech. Eng. **198**(49–52), 3902–3914 (2009)
13. Auricchio, F., Beirão da Veiga, L., Hughes, T.J.R., Reali, A., Sangalli, G.: Isogeometric collocation for elastostatics and explicit dynamics. Comput. Methods Appl. Mech. Eng. **249–252**, 2–14 (2012)
14. Auricchio, F., Beirão da Veiga, L., Kiendl, J., Lovadina, C., Reali, A.: Locking-free isogeometric collocation methods for spatial Timoshenko rods. Comput. Methods Appl. Mech. Eng. **263**, 113–126 (2013)
15. Bouclier, R., Elguedj, T., Combescure, A.: Locking free isogeometric formulations of curved thick beams. Comput. Methods Appl. Mech. Eng. **245–246**, 144–162 (2012)
16. Greco, L., Cuomo, M.: B-Spline interpolation of Kirchhoff–Love space rods. Comput. Methods Appl. Mech. Eng. **256**, 251–269 (2013)
17. Greco, L., Cuomo, M.: An implicit G^1 multi patch B-spline interpolation for Kirchhoff–Love space rod. Comput. Methods Appl. Mech. Eng. **269**, 173–197 (2014)
18. Beirão da Veiga, L., Lovadina, C., Reali, A.: Avoiding shear locking for the Timoshenko beam problem via isogeometric collocation methods. Comput. Methods Appl. Mech. Eng. **241–244**, 38–51 (2012)
19. Cazzani, A., Malagù, M., Stochino, F., Turco, E.: Constitutive models for strongly curved beams in the frame of isogeometric analysis. Math. Mech. Solids (2014, in press)
20. Cazzani, A., Malagù, M., Turco, E.: Isogeometric analysis of plane curved beams. Math. Mech. Solids. doi:10.1177/1081286514531265 (2014)
21. Pignataro, M., Luongo, A.: Asymmetric interactive buckling of thin-walled columns with initial imperfections. Thin-Walled Struct. **5**(5), 365–382 (1987)
22. Luongo, A.: Mode localization in dynamics and buckling of linear imperfect continuous structures. Nonlinear Dyn. **25**(1–3), 133–156 (2001)
23. Luongo, A.: On the amplitude modulation and localization phenomena in interactive buckling problems. Int. J. Solids Struct. **27**(15), 1943–1954 (1991)
24. Pignataro, M., Luongo, A., Rizzi, N.: On the effect of the local overall interaction on the postbuckling of uniformly compressed channels. Thin-Walled Struct. **3**(4), 293–321 (1985)
25. Piegl, L., Tiller, W.: The NURBS Book, 2nd edn. Springer, Berlin (1997)
26. Heyman, J.: The stone skeleton. Int. J. Solids Struct. **2**, 249–279 (1966)
27. Heyman, J.: The safety of masonry arches. Int. J. Mech. Sci. **11**, 363–385 (1969)
28. Heyman, J.: The Masonry Arch. Hellis Horwood, Chichester (1982)
29. Roca, P., Cervera, M., Gariup, G., Pela, L.: Structural analysis of masonry historical constructions. Eng. Struct. **17**, 299–325 (2007)
30. Tralli, A., Alessandri, C., Milani, G.: Computational methods for masonry vaults: a review of recent results. Open J. Civ. Eng. **8**, 272–287 (2014)
31. de Falco, C., Reali, A., Vazquez, R.: GeoPDEs: a research tool for isogeometric analysis of PDEs. Adv. Eng. Softw. **42**(12), 1020–1034 (2011)
32. Carandell, J.M., Vivas, P.: La Pedrera: A Work of Total Art. Triangle Postals, Barcelona (2002)
33. Huerta, S.: Structural design in the work of Gaudí. Archit. Sci. Rev. **49**, 324–339 (2006)
34. Benvenuto, E.: An Introduction to the History of Structural Mechanics. Part II: Vaulted Structures and Elastic Systems. Springer, New York (1991)
35. Huerta, S.: Mechanics of masonry vaults: the equilibrium approach. In: Lourenço, P.B., Roca, P. (eds.) Historical Constructions, pp. 47–69. Guimarães (2001)
36. Como, M.: Statics of Historic Masonry Constructions. Springer, Berlin (2013)
37. Chiozzi, A., Malagù, M., Tralli, A., Cazzani, A.: Isogeometric analysis of masonry arches: a simple applicative program (2014, submitted to J. Comput. Civil Eng.)
38. Rinaldi, A., Placidi, L.: A microscale second gradient approximation of the damage parameter of quasi-brittle heterogeneous lattices. ZAMM-Zeitschrift für Angewandte Mathematik und Mechanik. **1**(16) (2013). doi:10.1002/zamm.201300028
39. Rinaldi, A.: A rational model for 2D disordered lattices under uniaxial loading. Int. J. Damage Mech. **18**, 233–257 (2009)
40. Rinaldi, A.: Statistical model with two order parameters for ductile and statistical model with two order parameters for ductile and soft fiber bundles in nanoscience and biomaterials. Phys. Rev. E (Statistical, Nonlinear, and Soft Matter Physics), **83**, 046126(10) (2011)
41. Wang, Y., Zhang, T.: Finite element model updating using estimation of distribution algorithms. In: The 6th International Conference on Structural Health Monitoring of Intelligent Infrastructure (20013)

42. Wang, Y., Hao, H.: Damage identification scheme based on compressive sensing J. Comput. Civil Eng. (2014). doi:10.1061/(ASCE)CP.1943-5487.0000324
43. Eremeyev, V.A., Pietraszkiewicz, W.: The nonlinear theory of elastic shells with phase transitions. J. Elast. **74**(1), 67–86 (2004)
44. Yeremeyev, V.A., Freidin, A.B., Sharipova, L.L.: The stability of the equilibrium of two-phase elastic solids. J. Appl. Math. Mech. **71**(1), 61–84 (2007)
45. Eremeev, V.A., Freidin, A.B., Sharipova, L.L.: Nonuniqueness and stability in problems of equilibrium of elastic two-phase bodies. Dokl. Phys. **48**(7), 359–363 (2003)
46. dell'Isola, F., Romano, A.: On the derivation of thermomechanical balance equations for continuous systems with a nonmaterial interface. Int. J. Eng. Sci. **25**(11–12), 1459–1468 (1987)
47. D'Annibale, F., Luongo, A.: A damage constitutive model for sliding friction coupled to wear. Contin. Mech. Thermodyn. **25**(2–4), 503–522 (2013)
48. dell'Isola, F., Madeo, A., Seppecher, P.: Boundary conditions at fluid-permeable interfaces in porous media: a variational approach. Int. J. Solids Struct. **46**(17), 3150–3164 (2009)
49. dell'Isola, F., Seppecher, P., Madeo, A.: How contact interactions may depend on the shape of cauchy cuts in n-th gradient continua: approach á la D'Alembert. Zeitschrift für Angewandte Mathematik Und Physik (ZAMP) **63**(6), 1119–1141 (2012)
50. dell'Isola, F., Seppecher, P.: The relationship between edge contact forces, double forces and interstitial working allowed by the principle of virtual power. Comptes Rendus de l'Academie de Sciences-Serie IIb: Mecanique, Physique, Chimie, Astronomie **321**, 303–308 (1995)
51. Federico, S., Grillo, A., Imatani, S., Giaquinta, G., Herzog, W.: An energetic approach to the analysis of anisotropic hyperelastic materials. Int. J. Eng. Sci. **46**, 164–181 (2008)
52. Misra, A.: Mechanistic model for contact between rough surfaces. J. Eng. Mech. **123**(5), 475–484 (1997)
53. Roveri, N., Carcaterra, A.: Damage detection in structures under travelling loads by the Hilbert–Huang transform. Mech. Syst. Signal Process. **28**, 128–144 (2012)
54. Ferretti, M., Piccardo, G.: Dynamic modeling of taut strings carrying a traveling mass. Contin. Mech. Thermodyn. **25**(2–4), 469–488 (2013)
55. Contro, R., Poggi, C., Cazzani, A.: Numerical analysis of fire effects on beam structures. Eng. Comput. **5**, 53–58 (1988)
56. Cazzani, A., Contro, R., Corradi, L.: On the evaluation of the shakedown boundary for temperature-dependent elastic properties. Eur. J. Mech. A/Solids **11**, 539–550 (1992)
57. Andreaus, U., Baragatti, P.: Cracked beam identification by numerically analysing the nonlinear behaviour of the harmonically forced response. J. Sound Vib. **330**(4), 721–742 (2011)
58. Cazzani, A., Rovati, M.: Sensitivity analysis and optimum design of elastic-plastic structural systems. Meccanica **26**, 173–178 (1991)
59. Turco, E., Caracciolo, P.: Elasto-plastic analysis of Kirchhoff plates by high simplicity finite elements. Comput. Methods Appl. Mech. Eng. **190**, 691–706 (2000)
60. Neff, P., Sysow, A., Wieners, C.: Numerical approximation of incremental infinitesimal gradient plasticity. Int. J. Numer. Methods Eng. **77**, 414–436 (2009)